 FDMP, vol.14, no.1, pp.23-37, 2018

Numerical Visualizations of Mixing Enhancement in a 2D Supersonic Ejector

M. Dandani[1, *], V. Lepiller[2], A. Ghezal[3] and P. Desevaux[4]

Abstract: The present study deals with the numerical visualization of the mixing process in a 2D supersonic ejector. The mixing process is visualized using two CFD flow visualization methods. The first method consists in introducing discrete particles in the secondary flow and computing their trajectories. The second method consists in modeling the diffusion of a passive scalar introduced in one of the two flows. The mixing process is investigated in the case of a conventional 2D supersonic ejector and a second case of an ejector equipped with transverse micro jets. Flow visualizations obtained show the existence of a significant mixing enhancement when the ejector mixing chamber is equipped with wall slot injectors.

Keywords: Ejector, supersonic flow, mixing, active control, CFD.

1 Introduction

Supersonic ejectors are flow devices of rugged and simple construction, used to convert pressure energy into kinetic energy [Addy, Dutton and Mikkelsen (1981)]. They are usually made of two coaxial nozzles. The primary nozzle is designed to deliver a supersonic jet which sucks and entrains a secondary flow along the mixing chamber of the secondary nozzle. Supersonic ejectors are employed in a large variety of applications including vacuum pump, thermocompressor, static mixer, jet propulsion thrust augmentation systems, hydrogen recirculation in fuel cell. In all these applications, the role of the ejector is to suck, to entrain, to recompress and to mix two fluids.

The fluid mixing process remains not well known and researches for obtaining rapid mixing of two high speed streams in a short distance are very active [Gutmark, Schadow and Yu (1995); Seiner, Dash and Kenzakowski (2001)]. Among the passive techniques, the use of cavities [Ganesh and Samitha (2013)], vortex generating tabs [Hari and Kurian (2001)] and especially lobed nozzles [Rao and Jagadeesh (2014)] are the most common techniques used to enhance the mixing of two high speed flows.

[1] LMFTA, USTHB, Algiers, Algeria.

[2] FEMTO-ST-UMR 6174, Energy Dept, University of Bourgogne Franche-Comté, Belfort F-90000, France.

[3] LMFTA, USTHB, Algiers, Algeria.

[4] FEMTO-ST-UMR 6174, Energy Dept, University of Bourgogne Franche-Comté, Belfort F-90000, France.

* Corresponding author: M. Dandani. Email: Moundir.dandani@gmail.com.

Among the active techniques including counter jet suction, acoustic perturbations, the use of transverse jets is an ongoing technique which draws the attention of many researchers [Hidetaka, Hisashi, Myeong-Kwan et al. (2002); Zhang, Liu and Wang (2015); Huang (2016)]. However, it remains difficult to assess the quality of the mixing process. This can be investigated, qualitatively, thanks to flow visualization methods.

Experimentally, the most commonly used technique is the Laser Induced Fluorescence imaging technique (LIF) which allows good local characterization of the mixing and non-mixing regions [Desevaux (2001); Hu and Koochesfahani (2002)]. The laser tomography technique based on Mie scattering was also used by several authors [Rao and Jagadeesh (2014); Bouhanguel, Desevaux and Gavignet (2011)] to study the mixing process in supersonic flows.

Numerical approaches to study the mixing process in supersonic flows are less numerous. However, the progress made in the field of CFD has recently yielded very promising results thanks to Large Eddy Simulations [Le Ribault (2008); Bouhanguel, Desevaux and Gavignet (2015)].

Moreover, the flow region before the complete mixing (called the non-mixing zone) can be investigated by visual differentiation of the primary and secondary flows. Numerically, the differentiation between the two flows can be obtained by introducing discrete particles into the induced flow and by computing the particle trajectories [Desevaux and Aeschbacher (2002)]. Another numerical method consists in modeling the diffusion of a passive scalar introduced in one of the two flows [Bartosiewicz, Aidoun, Desevaux et al. (2005)]. These numerical flow visualizations have been used successfully by the present authors for visualizing the mixing process in cylindrical ejectors [Desevaux and Aeschbacher (2002)].

The work presented here is consists in using these numerical tools to visualize the mixing process between the motive and induced flows into 2D ejectors. The effects of transverse jets on the flow mixing are investigated.

2 Ejector geometry and mixing enhancement solution

The ejector considered in this work is made of two planar 2D nozzles as shown in Fig. 1. The main dimensions are indicated in this figure. The primary nozzle can deliver a supersonic jet with an exit Mach number of 1.82. The geometrical ratio of the ejector (i.e. ratio of the mixing chamber section on the primary nozzle throat section) is A=3. The mixing chamber is equipped with three wall slots arranged in staggered rows as shown in Fig. 1. These slots have a width h=1 mm and are used to deliver continuous transverse jets normally to the direction of the main flow.

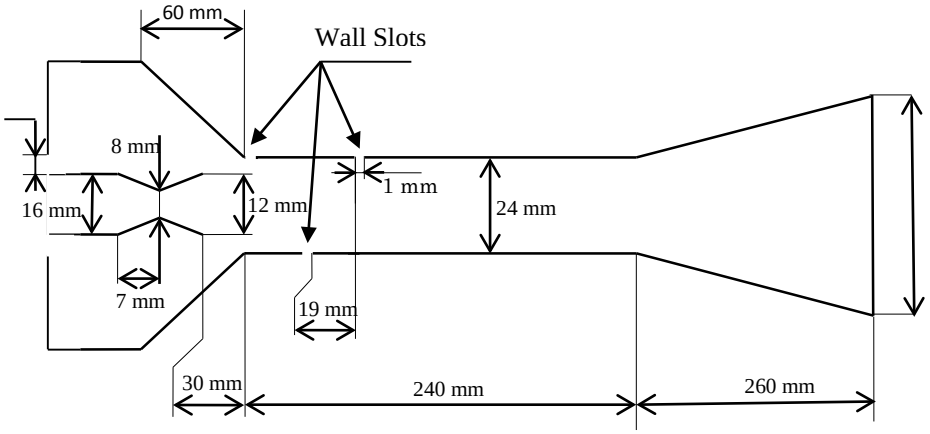

Figure 1: 2D ejector geometry

3 CFD approach

3.1 Governing equations

The flow in the ejector is governed by the compressible steady state form of the fluid flow conservation equations. The thermodynamics and transport properties for air are held constant. The trajectory of a discrete phase particles is predicted by integrating the force balance on the particle, which is written in a Lagrangian reference frame. This force balance equates the particle inertia with the forces acting on the particle. The momentum transfer from the continuous phase to the discrete phase is computed by examining the change in momentum of a particle as it passes through each control volume in the Ansys-Fluent model. This momentum exchange appears as a momentum source in the continuous phase momentum balance in any subsequent calculations of the continuous phase flow field.

The governing equations for the flow in the ejector can be written in their compact Cartesian form as follow:

Continuity equation

$$\frac{\partial \rho}{\partial t} + \frac{\partial}{\partial x_i}(\rho u_i) = 0 \tag{1}$$

Momentum equation

$$\frac{\partial \rho u_i}{\partial t} + \frac{\partial \rho u_i u_j}{\partial x_j} = -\frac{\partial P}{\partial x_i} + \frac{\partial \tau_{ij}}{\partial x_j} + S_m \tag{2}$$

Energy equation

$$\frac{\partial \rho E}{\partial t} + \frac{\partial}{\partial x_i}\big(u_i(\rho E + P)\big) = \vec{\nabla}\left(\alpha \frac{\partial T}{\partial t} + u_j(\tau_{ij})\right) + S_e \tag{3}$$

Where

$$\tau_{ij} = \mu_t \left(\frac{\partial u_i}{\partial x_j} + \frac{\partial u_j}{\partial x_i}\right) - \frac{2}{3}\mu_t \frac{\partial u_k}{\partial x_k}\delta_{ij} \tag{4}$$

S_m and S_e are the source terms for the discrete phase, which represent the integrated effects of the momentum and energy exchange with the continuous phase respectively.

They are expressed as follow:

$$S_m = m_p \frac{du_p}{dt} \tag{5}$$

$$S_e = m_p \frac{dT_p}{dt} \tag{6}$$

In the discrete phase model (DPM) the continuous phase is treated as a continuum, while the dispersed phase is solved by tracking a large number of spherical particles. The dispersed phase can exchange momentum, mass and energy with the base fluid. A fundamental assumption made in this model is that the dispersed phase is sufficiently dilute such that particle-particle interaction is almost negligible [Albojamal and Vafai (2017)]. By neglecting the effect of the discrete phase on the continuous phase, the discrete phase pattern is predicted based on a fixed continuous phase flow field (One-way coupling).

The equation of motion of the particle is given by the following equation:

$$\frac{\partial \vec{u}_p}{\partial t} = F_D\left(\vec{u} - \vec{u}_p\right) + \frac{\vec{g}(\rho_p - \rho)}{\rho_p} + \vec{F} \tag{7}$$

Where $F_D\left(u - u_p\right)$ is the drag (force/unit particle mass), which is exerted on the particles by the flow in the ejector and are carried with the flow. This drag force is calculated by the following relation:

$$F_D = \frac{18\mu}{\rho_p d_p^2} . \frac{C_D Re}{24} \tag{8}$$

$\vec{F}$ is an additional acceleration (force/unit particle mass)

Here, u is the fluid phase velocity, u_p and T_p are the particle velocity and temperature respectively, μ is the molecular viscosity of the fluid, ρ is the fluid density, ρ_p is the density of the particle, d_p is the particle diameter, and C_D is the drag coefficient. Re is the relative Reynolds number, which is defined as:

$$Re = \rho d_p \frac{|\vec{u}_p - \vec{u}|}{\mu} \tag{9}$$

3.2 Turbulence modeling

Regarding the modeling of the turbulence, a preliminary study has shown that RANS turbulence models were appropriate to simulate adequately flow phenomena in dry air powered ejectors [Desevaux, Marynowski and Khan (2006)]. Three RANS turbulence models are used in the present study: the standard *k-ε*, standard *k-ω* and SST *k-ω* models.

The *standard k-ε* model is based on transport equations for the turbulence kinetic energy *k* and its dissipation rate *ε*. *k* and *ε* are obtained from the following transport equations :

$$\frac{\partial}{\partial t}(pk) + \frac{\partial}{\partial x_i}(\rho k u_i) = \frac{\partial}{\partial x_i}\left[\left(\mu + \frac{\mu_t}{\sigma_k}\right)\frac{\partial k}{\partial x_i}\right] + G_k - \rho\epsilon - Y_M \tag{10}$$

$$\frac{\partial}{\partial t}(p\epsilon) + \frac{\partial}{\partial x_i}(\rho \epsilon u_i) = \frac{\partial}{\partial x_i}\left[\left(\mu + \frac{\mu_t}{\sigma_\epsilon}\right)\frac{\partial \epsilon}{\partial x_i}\right] + C_{1\epsilon}\frac{\epsilon}{k}G_k - C_{2\epsilon}\rho\frac{\epsilon^2}{k} \tag{11}$$

In these equations, G_k represents the generation of turbulent kinetic energy due to the mean velocity gradients. Y_M represents the contribution of the fluctuating dilatation in compressible turbulence to the overall dissipation rate. σ_k and σ_ε are the turbulent Prandtl numbers for k and ε, respectively. The turbulent viscosity μ_t is computed by combining k and ε:

$$\mu_t = \rho C_\mu \frac{k^2}{\epsilon} \tag{12}$$

The constants have the default values: $C_{1\varepsilon}$=1.44; $C_{2\varepsilon}$=1.92; C_μ=0.09; σ_k=1; σ_ε=1.3.

The *standard k-ω* model consists in replacing the equation for epsilon by a transport equation for the dissipation rate ω wich can also be though as the ratio $\frac{\epsilon}{k}$. The resulting equations are:

$$\frac{\partial}{\partial t}(pk) + \frac{\partial}{\partial x_i}(\rho k u_i) = \frac{\partial}{\partial x_i}\left[\left(\mu + \frac{\mu_t}{\sigma_k}\right)\frac{\partial k}{\partial x_i}\right] + G_k - Y_k \tag{13}$$

$$\frac{\partial}{\partial t}(p\omega) + \frac{\partial}{\partial x_i}(\rho \omega u_i) = \frac{\partial}{\partial x_i}\left[\left(\mu + \frac{\mu_t}{\sigma_\omega}\right)\frac{\partial \omega}{\partial x_i}\right] + G_\omega - \mathrm{Y}_\omega \tag{14}$$

Where G_k and G_ω are the generation for k and ω respectively. Y_k and Y_ω are the dissipation for k and ω respectively. The turbulent viscosity is evaluated by combining k and ω:

$$\mu_t = \rho \alpha^* \frac{k}{\omega} \tag{15}$$

Where α^* a function of the turbulent Reynolds is number and is equal to 1 for high Reynolds number.

The *standard k-ω* model incorporates modifications for low-Reynolds number effects, compressibility, and shear flow spreading. One of the weak points of this model is the sensitivity of the solutions to values for k and ω outside the shear layer (freestream sensitivity).

The *shear-stress transport (SST) k-ω* model was developed to effectively blend the robust and accurate formulation of the *k-ω* model in the near-wall region with the freestream independence of the *k-ε* model in the far field. To achieve this, the *SST k-ω* includes the addition of a cross-diffusion term in the ω equation and a blending function to ensure that the model equations behave appropriately in both near-wall and far-field zones. The resulting equations for k and ω are:

$$\frac{\partial}{\partial t}(pk) + \frac{\partial}{\partial x_i}(\rho k u_i) = \frac{\partial}{\partial x_i}\left[\left(\mu + \frac{\mu_t}{\sigma_k}\right)\frac{\partial k}{\partial x_i}\right] + G_k - Y_k \tag{16}$$

$$\frac{\partial}{\partial t}(p\omega) + \frac{\partial}{\partial x_i}(\rho \omega u_i) = \frac{\partial}{\partial x_i}\left[\left(\mu + \frac{\mu_t}{\sigma_\omega}\right)\frac{\partial \omega}{\partial x_i}\right] + G_\omega - \mathrm{Y}_\omega + D_\omega \tag{17}$$

3.3 Numerical method and conditions

The governing equations are solved using the commercial CFD package Ansys-Fluent. The flow studied here is highly compressible and supersonic. Shock waves that may form cause interdependence between density, pressure, energy and velocity. So we choose the coupled solver that solves the equations of continuity, momentum and energy simultaneously before solving the equations for turbulence and additional scalars.

The convective terms are discretized using a second-order upwind scheme and gradients are evaluated using the Green-Gauss node based approach.

The fluid used is air considered as an ideal gas.

The computational domain and the boundary conditions used in the present study are presented in Fig. 2.

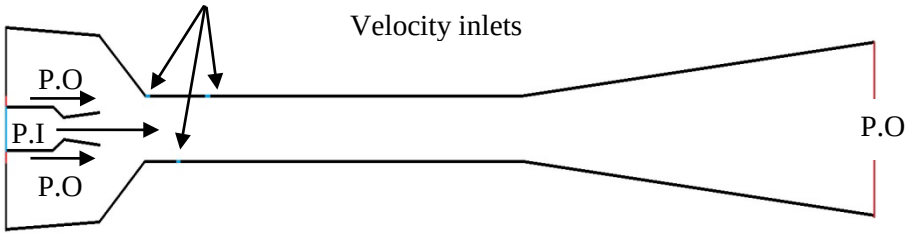

Figure 2: Computational domain with boundary conditions

P.O: Pressure Outlet; P.I: Pressure Inlet

A stagnation pressure is imposed at the inlet section of the primary nozzle, and the pressure at the outlet section of the ejector is fixed to the atmospheric pressure. A pressure outlet condition equal to the atmospheric pressure is imposed at the secondary flow inlet. Velocity inlet conditions are set at the transverse jet entrances.

Regarding the numerical convergence, a calculation is considered converged when the mass, momentum, energy and turbulence equations are balanced (i.e. when residues are stable and below 10^{-5}), when the total mass flow difference between inlets and outlet is less than 0.01% and also and when the induced mass flow rate reaches a stable value.

3.4 Mesh independence study

A mesh independence study was carried out using four different mesh grids. The main characteristics of the meshes used and the calculation time per iteration are summarized in Tab.1.

Table 1: Grid independence study

Grid	1	2	3	4
Cell size	1.5 mm	1 mm	0.5 mm	0.3 mm
Cell number	44000	54000	214700	575000
Calculation time / iteration	0.2 s	0.66 s	2.2 s	4.5 s

The centerline static pressure distribution is checked during the independence study. Fig. 3 presents results obtained for two values of the primary stagnation pressure P1 (3 and 4 bar). A very small difference for the four grids tested can be observed. Therefore, grid 1, which gives reduced calculation times, is used for the rest of this work.

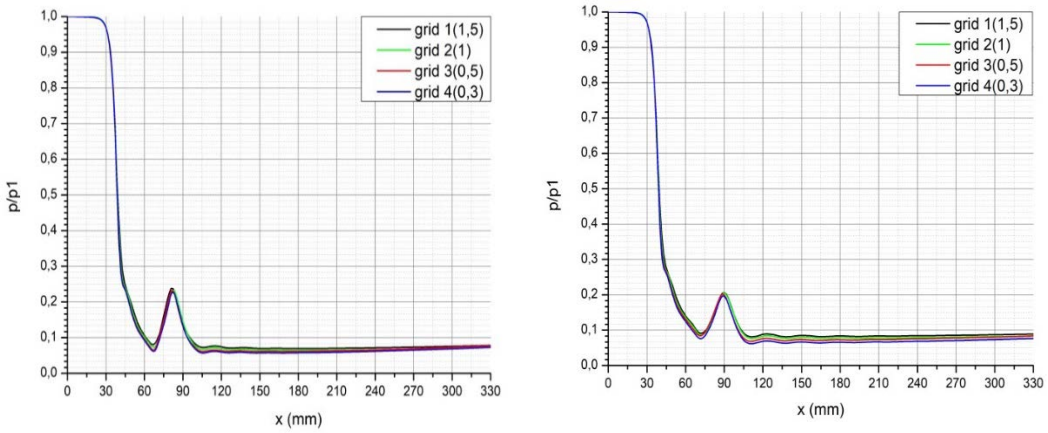

Figure 3: Centerline static pressure distributions obtained for different mesh grids

Fig. 4 shows the mesh grid on a part of the computational domain. A total of 44000 quadrilaterals cells are used to mesh the entire geometry.

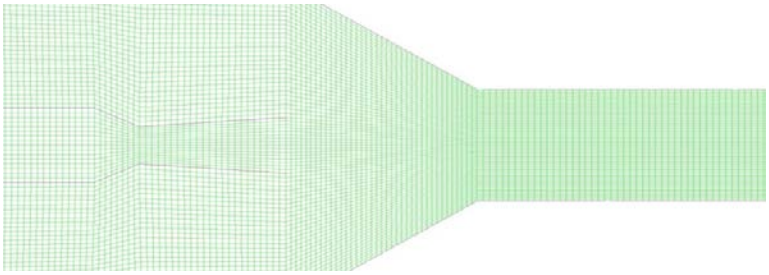

Figure 4: Mesh grid of a part of the computational domain

3.5 Preliminary validation of the CFD model

The validation of the CFD simulations was realized during a preliminary study carried out on the ejector of cylindrical section equipping our test bench [Desevaux, Bouhanguel, Girardot et al. (2013)]. The cylindrical ejector consists of two coaxial nozzles. Its geometrical ratio (i.e. ratio of the mixing chamber section on the primary nozzle throat section) is A=9 and the primary nozzle exit Mach number is equal to 2.33.

A measurement device was specifically designed to measure the static pressure on the axis of the ejector [Bouhanguel, Desevaux and Khan (2014)]. The centerline distributions of the static pressure were compared with those obtained numerically with a 2D axisymmetric CFD model and using different turbulence models. This comparison was made for two values of the primary stagnation pressure P1 (3 and 4 bar) and is presented in Fig. 4. Under these operating pressure conditions, the flow within the ejector is characterized by the formation of an oblique shock train at the outlet of the primary nozzle, which then attenuates in the mixing chamber. The ejector then operates in a mixed flow regime corresponding to a supersonic primary flow at the outlet of the motive

nozzle and a secondary flow which remains subsonic along the secondary nozzle. Fig. 4 shows a good agreement between the numerical and experimental results. Three RANS turbulence models are compared: the standard k-ε, standard k-ω and SST k-ω models. It is shown that the standard k-epsilon model gives results closest to experiments, in particular regarding the number of oblique shocks and their intensity, confirming results obtained previously [Desevaux, Marynowski and Khan (2006)].

Consequently, it is the standard k-ε model that will be used in the rest of this study for the simulation of the flow in 2D ejectors

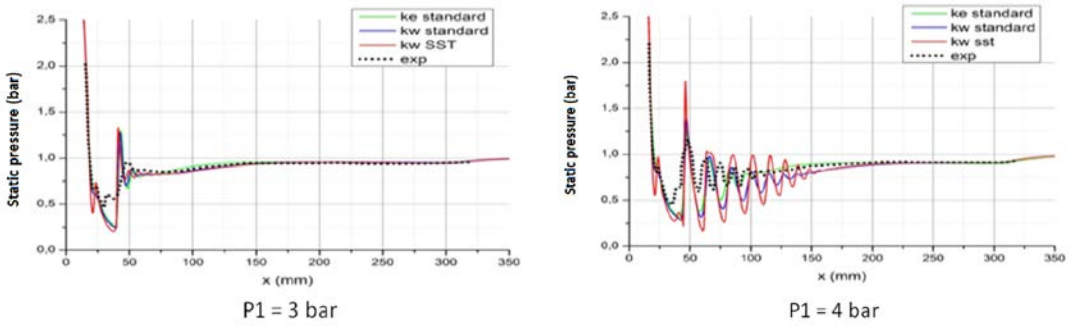

Figure 5: Experimental and CFD centerline pressure distributions in the case of a cylindrical ejector for two values of primary stagnation pressure

4 Results and discussion

4.1 Comparison of computed mass flow rates

Tab. 2 summarizes the values of the different mass flow rates (primary, induced and injected through the wall slots) computed for three values of the primary stagnation pressure P_1. For the transverse jets, three values of entrance velocity are considered: V=0, 100 and 150 m/s.

Table 2: Computed values of mass flow rates

		V=0 m/s	V=100 m/s	V=150 m/s
P_1=2 b	Primary mass flow rate	3.72 kg/s	3.72 kg/s	3.72 kg/s
	Induced mass flow rate	1.88 kg/s	1.86 kg/s	1.80 kg/s
	Transverse jets mass flow rate	0 kg/s	0.074 kg/s	0.12 kg/s
P_1=3 b	Primary mass flow rate	5.58 kg/s	5.58 kg/s	5.58 kg/s
	Induced mass flow rate	1.88 kg/s	1.85 kg/s	1.80 kg/s
	Transverse jets mass flow rate	0 kg/s	0.073 kg/s	0.11 kg/s
P_1=5 b	Primary mass flow rate	9.31 kg/s	9.31 kg/s	9.31 kg/s
	Induced mass flow rate	1.82 kg/s	1.72 kg/s	1.66 kg/s
	Transverse jets mass flow rate	0 kg/s	0.089 kg/s	0.14 kg/s

First, it is logically found that the wall injections have no effect on the primary mass flow. On the other hand, they tend to slightly reduce the induced flow rate. In all cases, the value of the total flow injected through the wall slots remains negligible (less than 2%) compared to the main flow.

Simulations also show a decrease of the induced flow rate when the primary stagnation pressure P_1 increases to 5 bar.

4.2 Visualization of the shock structure

The set of visualizations Fig. 5 discussed first concerns the shock structure which takes place in the mixing chamber when the primary nozzle operates in supersonic regime. This figure shows the Iso-Mach number contours obtained for the three considered values of primary pressure, without and with parietal jets (V=0, 100 and 150 m/s). The CFD simulations indicate that the primary nozzle exit Mach number is equal to 1.80. This value is in good agreement with the theoretical value of 1.82.

By comparing the shock structures displayed in Fig. 6, we can observe different flow patterns depending on the primary stagnation pressure. At the lowest pressure value (P_1=2 bar), the ejector operates in the mixed flow regime. The motive jet is supersonic at the primary nozzle exit. It decelerates to subsonic velocity through a series of oblique shocks in the first part of the mixing chamber. The induced flow remains subsonic along the secondary nozzle why there is no choking of the secondary nozzle.

For higher primary pressures (P_1=3 and 5 bar), the flow in the mixing chamber is fully supersonic. At P_1=3 bar, the flow returns to subsonic conditions through a quasi-normal shock at the diffuser entrance. For the pressure of 5 bar, this shock gives way to a shock train causing a shock-induced separation in the diffuser.

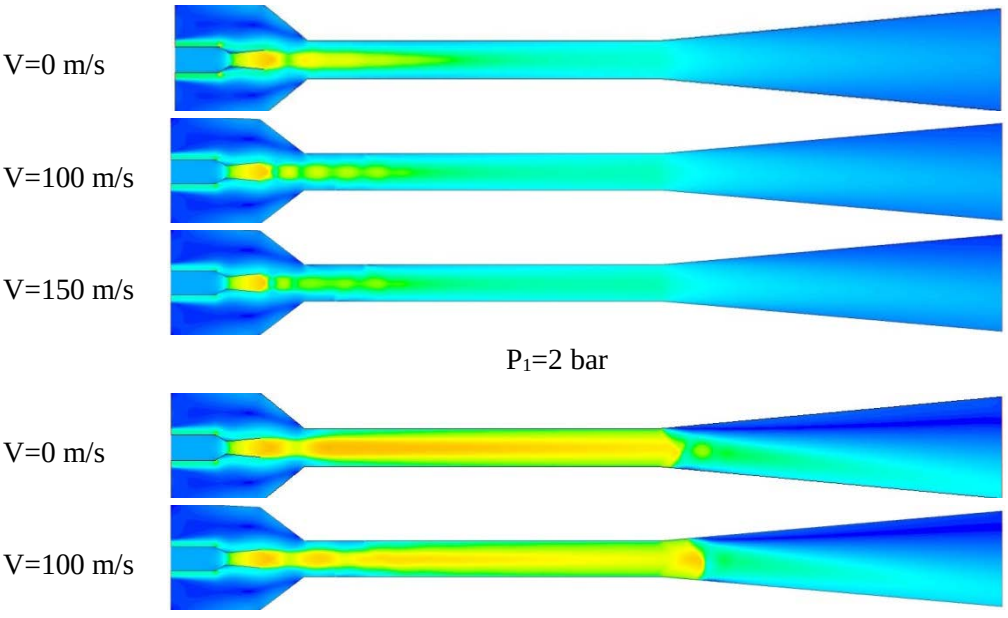

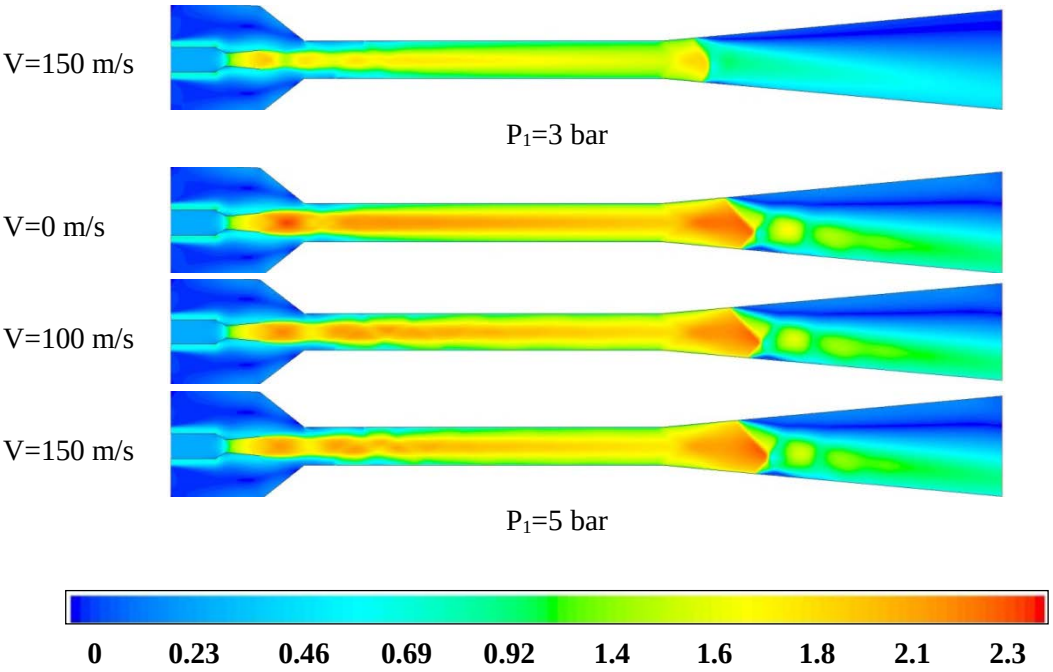

Figure 6 : Computational visualization of the shock structure Iso-Mach number contours

It is now well known that the optimal operating conditions for an ejector correspond to the transition between the mixed flow and fully supersonic regimes. This explains the degradation of the suction and entrainment performance observed in our simulations for the higher pressures, a decrease of approximately 8% of the induced mass flow rate when the primary pressure passes from 3-5 bar.

These flow visualizations clearly show the effects of the parietal injections on the shock structure in the mixing chamber. These effects increase with the increasing of the mass flow rate injected through the wall slots and cause the deformation of the shock structure. These transverse injections seem to have the effect of reducing the suction capacity of the ejector by delaying the establishment of the fully supersonic regime in the mixing chamber. This phenomenon is particularly visible on the flow visualizations corresponding to the primary pressure of 3 bar.

4.3 Visualization of the mixing process

The Iso-Mach number contours are very useful for analyzing the shock structure and the flow pattern but do not permit the mixing process between the primary and secondary flows to be investigated. A CFD procedure using numerical tracers [Desevaux and Aeschbacher (2002)] is used. This procedure consists in introducing liquid micro droplets (droplet diameter=1 μm) into the secondary flow and in predicting the particles trajectories by taking into account the effect of the continuous phase turbulence on the dispersion of the particles. This method permits the visualization of the secondary flow and the mixing region between the primary and the secondary flows Fig. 6. The non-mixing region, formed by the primary jet only, appears as white.

The flow visualizations displayed in Fig. 7 shows, as expected, a significant lengthening of the non-mixing region with increasing the primary stagnation pressure. In addition, the tracking of the particles trajectories confirms the strong separation of the flow in the diffuser caused by the shock at the diffuser entrance.

Regarding the influence of the parietal injections on the mixing, it seems to be almost negligible for the primary pressure of 2 bar. On the other hand, the use of these parietal jets leads to a significant decrease in the non-mixing length for higher values of primary pressure, indicating an improvement of the mixing process between the primary and induced flows.

Fig. 8 presents mixing flow visualizations performed using the second computational flow visualization method which consists in modeling the diffusion of a passive scalar introduced in one of the two flows. In the case of Fig. 7, the passive scalar, where the scalar concentration equals to 1, is introduced in the induced flow. The non-mixing region, formed by the primary jet only, appears as black where scalar concentration equal to 0.

The visualizations obtained confirm the results obtained using the discrete particles. Furthermore, the flow visualizations related to the primary pressure of 5 bar show a small deformation of the shape of the non-mixing region which is probably caused by the interaction of the main supersonic flow with the transverse jets.

It may be also noted that this visualization method has the benefit of quantifying the mixing process by following the evolution of the scalar concentration within the flow. It is thus seen that the mixing is not homogeneous along the mixing chamber and that the mixing is very difficult to achieve in the core of the flow.

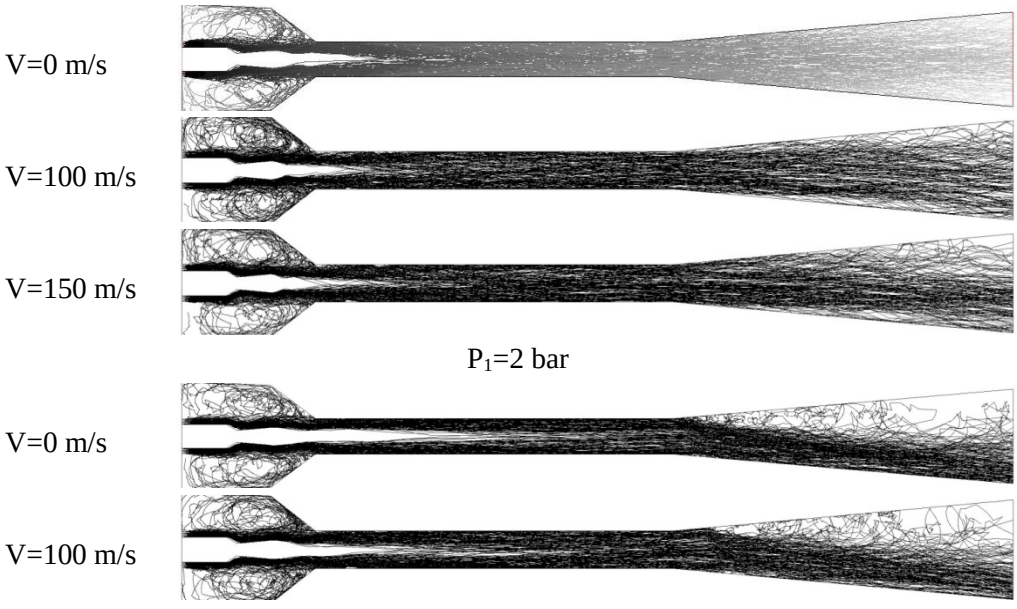

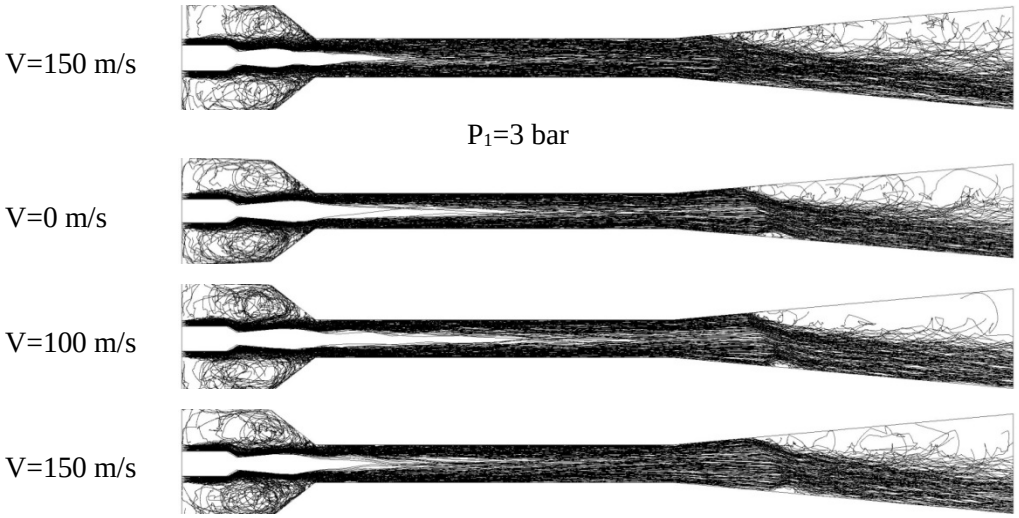

Figure 7: Computational visualization of the mixing process by introducing discrete tracers in the induced flow

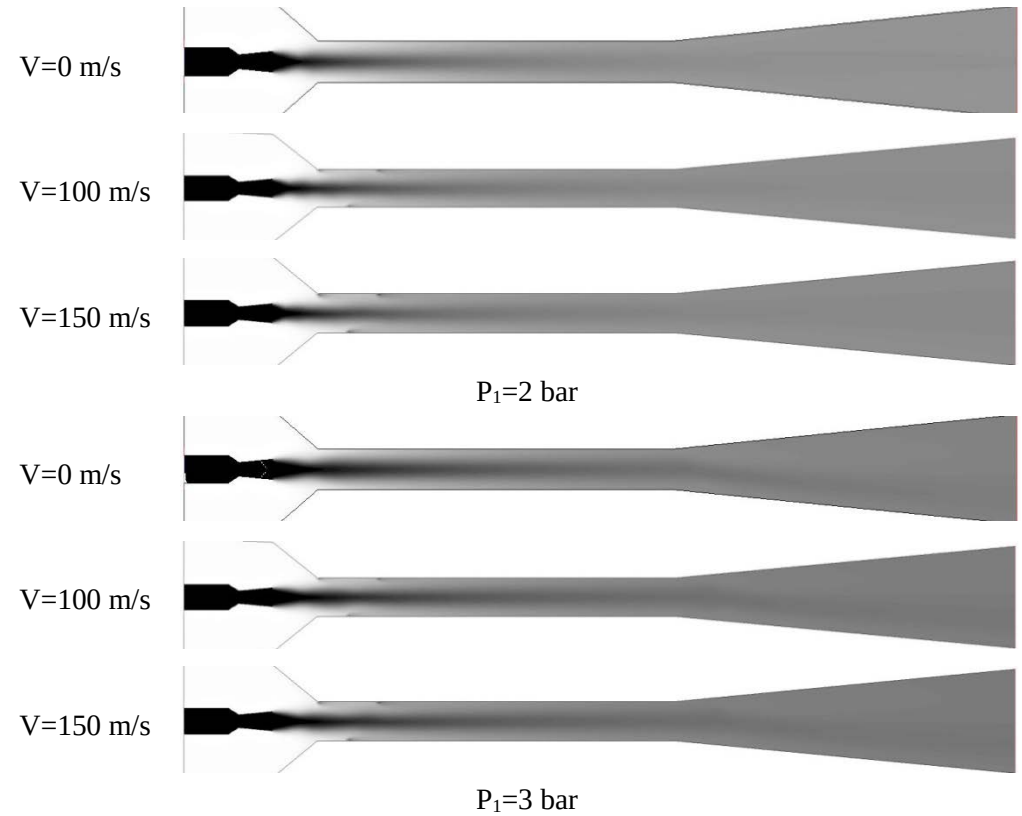

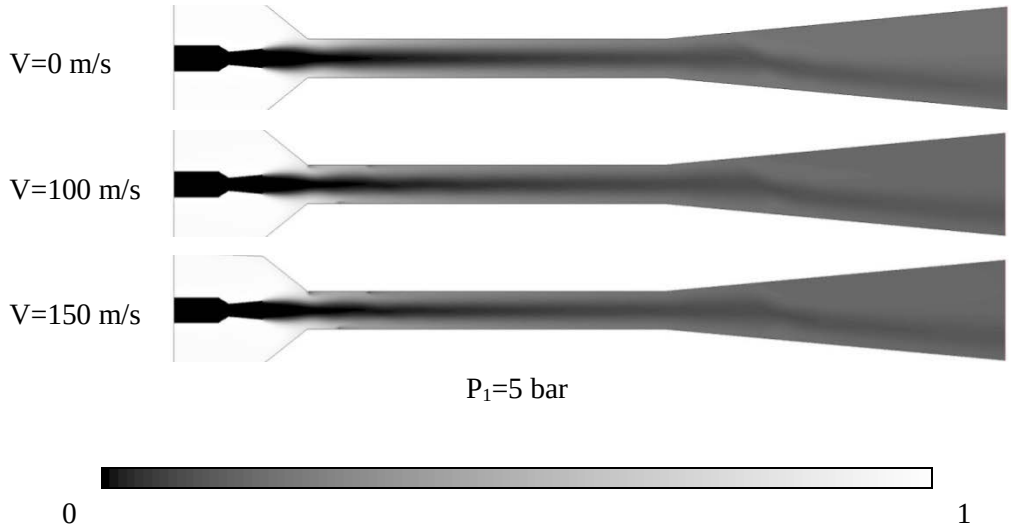

Figure 8: Computational visualization of the mixing process by introducing a passive scalar in the induced flow

5 Conclusion

This paper deals with the mixing enhancement inside 2D supersonic ejectors. In order to study the mixing process between the central core (primary) and annular (induced) flows, two CFD flow visualization methods are used:

- The first method consists in introducing discrete particles in the secondary flow and computing their trajectories,
- The second method consists in modeling the diffusion of a passive scalar introduced in the secondary flow.

Flow visualizations obtained during this work have shown significant mixing enhancement when the ejector mixing chamber is equipped with wall slot injectors.

These two methods, associated with more traditional CFD results, have shown that they could be effective numerical tools to predict the mixing process in supersonic ejectors, to investigate the mixing quality and to provide necessary understanding for the development of efficient mixing mechanisms.

Further work is underway to apply these numerical tools to the systematic investigation of the mixing enhancement by use of transverse jets (determination of the number, the dimension and the position of the slots, velocity of the transverse jets).

The use of pulsed transverse jets instead of continuous jets shall also be investigated through these methods using an unsteady CFD model.

Reference

Addy, A. L.; Dutton, J. C.; Mikkelsen, C. C. (1981): *Supersonic ejector-diffuser: theory and experiments*. University of Illinois, Urbana.

Albojamal, A.; Vafai, K. (2017): Analysis of single phase, discrete and mixture models, in predicting nanofluid transport. *International Journal of Heat and Mass Transfer*, vol. 114, pp. 225-237.

Bartosiewicz, Y.; Aidoun, Z.; Desevaux, P.; Mercadier, Y. (2005): Numerical and experimental investigations on supersonic ejectors. *International Journal of Heat and Fluid Flow*, vol. 26, pp. 56-70.

Bouhanguel, A.; Desevaux, P.; Gavignet, E. (2011): Flow visualization in supersonic ejectors using laser tomography techniques. *International journal of refrigeration*, vol. 34, pp. 1633-1640.

Bouhanguel, A.; Desevaux, P.; Gavignet, E. (2015): Visualization of flow instabilities in supersonic ejectors using Large Eddy Simulation. *Journal of Visual Communication and Image Representation*, vol. 18, pp. 17-19.

Bouhanguel, A; Desevaux, P.; Khan, M. (2014): Numerical design study of an axial probe for pressure measurement in supersonic air ejector. *15th International Symposium on Flow Visualization ISFV15*, Barcelona.

Desevaux P.; Aeschbacher, O. (2002): Numerical and experimental flow visualizations of the mixing process inside an induced air ejector. *International Journal of Turbo & Jet-Engines*, vol. 19, pp. 71-78.

Desevaux, P. (2001): A method for visualizing the mixing zone between two co-axial flows in an ejector. *Optics and Lasers in Engineering*, vol. 35, pp. 317-323.

Desevaux, P.; Bouhanguel, A.; Girardot, L.; Gavignet, E. (2013): On the use of laser tomography for validating CFD simulations of the flow in supersonic ejectors. *International Journal of Fluid Mechanics Research*, vol. 40, pp. 60-70.

Desevaux, P.; Marynowski, T.; Khan, M. (2006): CFD prediction of supersonic ejectors performance. *International Journal of Turbo & Jet-Engines*, vol. 23, pp. 173-181.

Ganesh, R; Samitha, Z. A. (2013): Mixing enhancement in supersonic coaxial flows with angle rear wall cavity using clover nozzle. *International Journal of Scientific and Engineering Research*, vol. 4, no. 8.

Gutmark, E.; Schadow, K.; Yu, K. (1995): Mixing enhancement in supersonic free shear flows. *Annual Review of Fluid Mechanics*, vol. 27, pp. 375-417.

Hari, S.; Kurian, J. (2001): Effectiveness of secondary tabs for supersonic mixing. *Experiments in Fluids*, vol. 32, pp. 302-308.

Hidetaka, O.; Hisashi, H.; Myeong-Kwan, P.; Shuzo, O.; Ryuichiro, Y. (2002): Control of pseudo-shock by slot injection. *Japan Society of Mechanical Engineers*, vol. 45, pp. 150-157.

Hu, H.; Koochesfahani, **M.** (2002): A novel method for instantaneous, quantitative measurement of molecular mixing in gaseous flows. *Experiments in Fluids*, vol. 33, no. 1, pp. 202-209.

Huang, W. (2016): Transverse jet in supersonic crossflows. *Aerospace Science and Technology*, vol. 50, pp. 183-195.

Le Ribault, C. (2008): Large eddy simulation of passive scalar in compressible mixing layers. *International Journal of Heat and Mass Transfer*, vol. 51, pp. 3514-3524.

Rao, S. M. V.; Jagadeesh, G. (2014): Novel supersonic nozzles for mixing enhancement in supersonic ejectors. *Applied Thermal Engineering*, vol. 71, pp. 62-71.

Seiner, J. M.; Dash, S. M.; Kenzakowski, D. C. (2001): Historical survey on enhanced mixing in scramjet engines. *Journal of Propulsion and Power*, vol. 17, pp. 1273-1286.

Zhang, Y.; Liu, W.; Wang, B. (2015): Effects of oblique and transverse injection on the characteristics of jet in supersonic crossflow. *Acta Astronaut*, vol. 115, pp. 256-366.